Determining the internal quantum efficiency of shallow-implanted nitrogen-vacancy defects in bulk diamond

Radko, Ilya; Boll, Mads; Israelsen, Niels Møller; Raatz, Nicole; Meijer, Jan; Jelezko, Fedor; Andersen, Ulrik Lund; Huck, Alexander

Published in:
Optics Express

Link to article, DOI:
10.1364/OE.24.027715

Publication date:
2016

Document Version
Publisher's PDF, also known as Version of record

Research Article | Vol. 24, No. 24 | 28 Nov 2016 | OPTICS EXPRESS 27715

Optics EXPRESS

Determining the internal quantum efficiency of shallow-implanted nitrogen-vacancy defects in bulk diamond

ILYA P. RADKO,[1,*] MADS BOLL,[1] NIELS M. ISRAELSEN[2] NICOLE RAATZ,[3] JAN MEIJER,[3] FEDOR JELEZKO,[4] ULRIK L. ANDERSEN,[1] AND ALEXANDER HUCK[1]

[1]*Department of Physics, Technical University of Denmark, 2800 Kongens Lyngby, Denmark*
[2]*Department of Photonics Engineering, Technical University of Denmark, 2800 Kongens Lyngby, Denmark*
[3]*Institute for Experimental Physics II, University of Leipzig, 04103 Leipzig, Germany*
[4]*Institute for Quantum Optics, Ulm University, 89073 Ulm, Germany*
[*]*iradko@fysik.dtu.dk*

Abstract: It is generally accepted that nitrogen-vacancy (NV) defects in bulk diamond are bright sources of luminescence. However, the exact value of their internal quantum efficiency (IQE) has not been measured so far. Here we use an implementation of Drexhage's scheme to quantify the IQE of shallow-implanted NV defects in a single-crystal bulk diamond. Using a spherical metallic mirror with a large radius of curvature compared to the optical spot size, we perform calibrated modifications of the local density of states around NV defects and observe the change of their total decay rate, which is further used for IQE quantification. We also show that at the excitation wavelength of 532 nm, photo-induced relaxation cannot be neglected even at moderate excitation powers well below the saturation level. For NV defects shallow implanted 4.5 ± 1 and 8 ± 2 nm below the diamond surface, we determine the quantum efficiency to be 0.70 ± 0.07 and 0.82 ± 0.08, respectively.

OCIS codes: (160.2220) Defect-center materials; (160.2540) Fluorescent and luminescent materials; (180.1790) Confocal microscopy.

References and links

1. C. Kurtsiefer, S. Mayer, P. Zarda, and H. Weinfurter, "Stable solid-state source of single photons," Phys. Rev. Lett. **85**, 290–293 (2000).
2. F. Jelezko and J. Wrachtrup, "Single defect centres in diamond: A review," Phys. Status Solidi **203**, 3207–3225 (2006).
3. B. B. Buckley, G. D. Fuchs, L. C. Bassett, and D. D. Awschalom, "Spin-light coherence for single-spin measurement and control in diamond," Science **330**, 1212–1215 (2010).
4. L. Robledo, L. Childress, H. Bernien, B. Hensen, P. F. A. Alkemade, and R. Hanson, "High-fidelity projective read-out of a solid-state spin quantum register," Nature **477**, 574–578 (2011).
5. G. Balasubramanian, P. Neumann, D. Twitchen, M. Markham, R. Kolesov, N. Mizuochi, J. Isoya, J. Achard, J. Beck, J. Tissler, V. Jacques, P. R. Hemmer, F. Jelezko, and J. Wrachtrup, "Ultralong spin coherence time in isotopically engineered diamond," Nat. Mater. **8**, 383–387 (2009).
6. V. N. Mochalin, O. Shenderova, D. Ho, and Y. Gogotsi, "The properties and applications of nanodiamonds," Nat. Nanotechnol. **7**, 11–23 (2012).
7. T. D. Ladd, F. Jelezko, R. Laflamme, Y. Nakamura, C. Monroe, and J. L. O'Brien, "Quantum computers," Nature **464**, 45–53 (2010).
8. P. Maletinsky, S. Hong, M. S. Grinolds, B. Hausmann, M. D. Lukin, R. L. Walsworth, M. Loncar, and A. Yacoby, "A robust scanning diamond sensor for nanoscale imaging with single nitrogen-vacancy centres," Nat. Nanotechnol. **7**, 320–324 (2012).
9. G. Balasubramanian, I. Y. Chan, R. Kolesov, M. Al-Hmoud, J. Tisler, C. Shin, C. Kim, A. Wojcik, P. R. Hemmer, A. Krueger, T. Hanke, A. Leitenstorfer, R. Bratschitsch, F. Jelezko, and J. Wrachtrup, "Nanoscale imaging magnetometry with diamond spins under ambient conditions," Nature **455**, 648–651 (2008).
10. J. R. Maze, P. L. Stanwix, J. S. Hodges, S. Hong, J. M. Taylor, P. Cappellaro, L. Jiang, M. V. Gurudev Dutt, E. Togan, A. S. Zibrov, A. Yacoby, R. L. Walsworth, and M. D. Lukin, "Nanoscale magnetic sensing with an individual electronic spin in diamond," Nature **455**, 644–647 (2008).

#279072 http://dx.doi.org/10.1364/OE.24.027715
Journal © 2016 Received 18 Oct 2016; revised 15 Nov 2016; accepted 15 Nov 2016; published 18 Nov 2016

Optics EXPRESS

11. J. M. Taylor, P. Cappellaro, L. Childress, L. Jiang, D. Budker, P. R. Hemmer, A. Yacoby, R. Walsworth, and M. D. Lukin, "High-sensitivity diamond magnetometer with nanoscale resolution," Nat. Phys. **4**, 810–816 (2008).
12. T. Wolf, P. Neumann, K. Nakamura, H. Sumiya, T. Ohshima, J. Isoya, and J. Wrachtrup, "Subpicotesla diamond magnetometry," Phys. Rev. X **5**, 041001 (2015).
13. F. Dolde, H. Fedder, M. W. Doherty, T. Nobauer, F. Rempp, G. Balasubramanian, T. Wolf, F. Reinhard, L. C. L. Hollenberg, F. Jelezko, and J. Wrachtrup, "Electric-field sensing using single diamond spins," Nat. Phys. **7**, 459–463 (2011).
14. G. Kucsko, P. C. Maurer, N. Y. Yao, M. Kubo, H. J. Noh, P. K. Lo, H. Park, and M. D. Lukin, "Nanometre-scale thermometry in a living cell," Nature **500**, 54–58 (2013).
15. A. Mohtashami and A. F. Koenderink, "Suitability of nanodiamond nitrogen-vacancy centers for spontaneous emission control experiments," New J. Phys. **15**, 043017 (2013).
16. L. Liebermeister, F. Petersen, A. V. Munchow, D. Burchardt, J. Hermelbracht, T. Tashima, A. W. Schell, O. Benson, T. Meinhardt, A. Krueger, A. Stiebeiner, A. Rauschenbeutel, H. Weinfurter, and M. Weber, "Tapered fiber coupling of single photons emitted by a deterministically positioned single nitrogen vacancy center," Appl. Phys. Lett. **104**, 031101 (2014).
17. K. H. Drexhage, "Influence of a dielectric interface on fluorescence decay time," J. Lumin. **1-2**, 693–701 (1970).
18. R. E. Kunz and W. Lukosz, "Changes in fluorescence lifetimes induced by variable optical environments," Phys. Rev. B **21**, 4814–4828 (1980).
19. B. C. Buchler, T. Kalkbrenner, C. Hettich, and V. Sandoghdar, "Measuring the quantum efficiency of the optical emission of single radiating dipoles using a scanning mirror," Phys. Rev. Lett. **95**, 063003 (2005).
20. A. I. Chizhik, A. M. Chizhik, D. Khoptyar, S. Bar, A. J. Meixner, and J. Enderlein, "Probing the radiative transition of single molecules with a tunable microresonator," Nano Lett. **11**, 1700–1703 (2011).
21. J. Johansen, S. Stobbe, I. S. Nikolaev, T. Lund-Hansen, P. T. Kristensen, J. M. Hvam, W. L. Vos, and P. Lodahl, "Size dependence of the wavefunction of self-assembled InAs quantum dots from time-resolved optical measurements," Phys. Rev. B **77**, 073303 (2008).
22. M. L. Andersen, S. Stobbe, A. S. Sorensen, and P. Lodahl, "Strongly modified plasmon-matter interaction with mesoscopic quantum emitters," Nat. Phys. **7**, 215–218 (2011).
23. P. Lunnemann, F. T. Rabouw, R. J. A. van Dijk-Moes, F. Pietra, D. Vanmaekelbergh, and A. F. Koenderink, "Calibrating and controlling the quantum efficiency distribution of inhomogeneously broadened quantum rods by using a mirror ball," ACS Nano **7**, 5984–5992 (2013).
24. B. K. Ofori-Okai, S. Pezzagna, K. Chang, M. Loretz, R. Schirhagl, Y. Tao, B. A. Moores, K. Groot-Berning, J. Meijer, and C. L. Degen, "Spin properties of very shallow nitrogen vacancy defects in diamond," Phys. Rev. B **86**, 081406(R) (2012).
25. M. Patting, M. Wahl, P. Kapusta, and R. Erdmann, "Dead-time effects in TCSPC data analysis," Proc. SPIE **6583**, 658307 (2007).
26. M. Pelton, "Modified spontaneous emission in nanophotonic structures," Nat. Photonics **9**, 427–435 (2015).
27. P. Ginzburg, "Cavity quantum electrodynamics in application to plasmonics and metamaterials," Rev. Phys. **1**, 120–139 (2016).
28. W. Lukosz and R. E. Kunz, "Light emission by magnetic and electric dipoles close to a plane interface," J. Opt. Soc. Am. **67**, 1607–1615 (1977).
29. R. R. Chance, A. Prock, and R. Silbey, "Molecular fluorescence and energy transfer near interfaces," Adv. Chem. Phys. **37**, 1–65 (1978).
30. R. R. Chance, A. H. Miller, A. Prock, and R. Silbey, "Fluorescence and energy transfer near interfaces: The complete and quantitative description of the Eu^{+3}/mirror systems," J. Chem. Phys. **63**, 1589–1595 (1975).
31. N. B. Manson, J. P. Harrison, "Photo-ionization of the nitrogen-vacancy center in diamond," Diamond Relat. Mater. **14**, 1705–1710 (2005).
32. G. Waldherr, J. Beck, M. Steiner, P. Neumann, A. Gali, T. Frauenheim, F. Jelezko, and J. Wrachtrup, "Dark states of single nitrogen-vacancy centers in diamond unraveled by single shot NMR," Phys. Rev. Lett. **106**, 157601 (2011).
33. N. Aslam, G. Waldherr, P. Neumann, F. Jelezko, and J. Wrachtrup, "Photo-induced ionization dynamics of the nitrogen vacancy defect in diamond investigated by single-shot charge state detection," New J. Phys. **15**, 013064 (2013).
34. A. T. Collins, M. F. Thomaz, and M. I. B. Jorge, "Luminescence decay time of the 1.945 eV centre in type Ib diamond," J. Phys. C **16**, 2177–2181 (1983).
35. A. Batalov, C. Zierl, T. Gaebel, P. Neumann, I.-Y. Chan, G. Balasubramanian, P. R. Hemmer, F. Jelezko, and J. Wrachtrup, "Temporal coherence of photons emitted by single nitrogen-vacancy defect centers in diamond using optical rabi-oscillations," Phys. Rev. Lett. **100**, 077401 (2008).
36. L. Robledo, H. Bernien, T. Sar, and R. Hanson, "Spin dynamics in the optical cycle of single nitrogen-vacancy centres in diamond," New J. Phys. **13**, 025013 (2011).
37. G. Davies and M. F. Hamer, "Optical studies of the 1.945 eV vibronic band in diamond," Proc. R. Soc. Lond. A Mat. **348**, 285–298 (1976).
38. F. Kaiser, V. Jacques, A. Batalov, P. Siyushev, F. Jelezko, and J. Wrachtrup, "Polarization properties of single photons emitted by nitrogen-vacancy defect in diamond at low temperature," arXiv:0906.3426.
39. P. B. Johnson and R. W. Christy, "Optical constants of transition metals: Ti, V, Cr, Mn, Fe, Co, Ni, and Pd," Phys.

Optics EXPRESS

Rev. B **9**, 5056–5070 (1974).

1. Introduction

Nitrogen-vacancy (NV) defects in diamond have proven to be a versatile instrument in quantum-optical technologies. Besides being an extremely stable source of single-photon luminescence that does not bleach [1], they also possess a paramagnetic ground state which can be optically initialized and readout [2–4]. Moreover, the coherence time of the associated electron-spin is extremely long [5], and the diamond host material itself has low cytotoxicity [6]. This unique set of properties makes NV centers in diamond a leading platform for quantum information processing [7] and a high precision optical sensor for magnetic- and electric fields as well as temperature [8–14]. All these applications rely on NV defects being stable and, most importantly, bright sources of luminescence. While the stability has been verified many times, the brightness can only be guaranteed by the high internal quantum efficiency (IQE), η, of the defect. The IQE is given as the ratio of the radiative emission rate, Γ_{rad}, to the total decay rate of the optically excited state: $\eta = \Gamma_{rad}/(\Gamma_{rad} + \Gamma_{nr})$. Since non-radiative decay rates, Γ_{nr}, cannot be accessed experimentally, it is not possible to measure the IQE directly.

There are few works that aim at quantifying the IQE of NV defects in diamond. Mohtashami and Koenderink [15] considered diamond nanocrystals containing native single NV defects, and found that for NV defects in 25-nm nanodiamonds the IQE is distributed between 0 and 20%, while for 100-nm nanodiamonds the IQE has an even larger distribution in the range 10–90%. The result for the smallest nanodiamonds is partially supported by fitting the measured second-order correlation function of a NV defect with that of a three-level system [16]. Interestingly, it was shown in [15] that the wide IQE distribution is due to a variation in both the radiative as well as the *non-radiative* decay rates among the different nanocrystals. This is surprising since the non-radiative rates are not of electromagnetic origin, therefore not sensitive to the local density of optical states (LDOS) and therefore the variation was due to intrinsic properties of the nanocrystals. Specifically, the lower IQE for 25-nm nanodiamonds is due to an enhanced Γ_{nr}, which is potentially associated with the increased nanocrystal surface-to-volume ratio and nanocrystal irregularities, such as local strain. In this respect, the IQE quantification of NV defects in bulk diamond is of large interest as it represents an “unperturbed” case and allows for the deduction of the IQE in highly relevant diamond geometries.

In this article, we report on a consistent measurement of the IQE of NV defects in bulk diamond through modification of their photonic environment (and hence the LDOS) with the use of a metallic mirror brought in close proximity to the defects. The total decay rate is given by $\Gamma_{tot} = \Gamma_{rad} + \Gamma_{nr}$. The central idea of our measurements is to controllably vary the radiative part Γ_{rad} by a calibrated modification of the LDOS, while the nonradiative part remains unchanged. By quantifying the change of the total decay rate Γ_{tot} as a response to the change in LDOS, we extract both terms and evaluate the IQE. We note that throughout this article unless explicitly stated differently we always refer to the negative charge state of NV defects in diamond.

The influence of a metal mirror and its separation from excited fluorescing dye molecules to their lifetime has been carefully studied in several pioneering experiments by Drexhage (e.g., see [17]). To precisely control the separation between the dye molecules and the mirror, he used the Langmuir-Blodgett dipping technique to deposit a varying number of layers of fatty acid on a metal surface. The same scheme, but with a number of improvements and modifications, has been used to characterize different types of quantum emitters: single molecules [18–20], self-assembled [21, 22] and colloidal [23] quantum dots, as well as NV defects in diamond nanocrystals [15]. In our work, we use an experimental approach that was first suggested in [19] and later modified for well calibrated measurements [15, 23]. The approach consists in using a scanning metallic mirror, so that the distance between an emitter and the mirror can be changed

Optics EXPRESS

in the course of the experiment, without the need to fabricate a new sample. By using a spherical mirror [15] the separation between a NV defect and the metal mirror can be precisely controlled by a lateral mirror displacement. This approach yields a nanometer-scale precision and will thus be used in this work. We limit our consideration to NV defects implanted with energies of 2.5 and 5 keV, resulting in a respective implantation depth of 4.5 and 8 nm below the diamond surface. From a set of reproducible measurements, we determine in our experiments the IQE to be 0.70 ± 0.07 and 0.82 ± 0.08 for 4.5 and 8 nm-deep NV defect ensembles, respectively.

2. Experimental arrangement

We use a commercial CVD grown electronic-grade single-crystalline diamond plate with a thickness of 0.3 mm from Element6 with a polished (100) top face. NV centers were implanted in circular areas of $\sim$ 250 ± 30 μm in diameter using a low-energy source of $^{15}N^{+}$ ions. The irradiation dose were determined to $D_{2.5keV} = (1.09 \pm 0.22) \cdot 10^{13}$ ions/cm^2 and $D_{5keV} = (1.53 \pm 0.32) \cdot 10^{13}$ ions/cm^2. Using the results of Monte Carlo simulations, the depth of ion implantation was estimated to be $h_{2.5keV} = 4.5 \pm 1$ nm and $h_{5keV} = 8 \pm 2$ nm for ions with an energy of 2.5 and 5 keV [24], respectively. After implantation, the samples were annealed in vacuum at 650 degrees Celsius yielding a nearly uniform two-dimensional distribution of NV defects. We confirmed the uniformity by recording confocal luminescence images of the implantation regions, which featured intensity fluctuations of less than 10%. Assuming a 1% conversion efficiency from $^{15}N^{+}$ ions to NV defects, we estimated the average distance between the latter to be about 35 nm. This separation is large enough to neglect dipole-dipole interactions between NV defects, and thus that in our experiment we probe an ensemble of individual non-interacting emitters.

The calibrated distance adjustment between the NV defects and the metallic mirror is achieved with the use of a spherical metal surface. For this purpose, we covered a 1-mm-radius hemisphere with a 400-nm-thick layer of titanium. Although titanium is less reflective than e.g. silver, it has the advantage of offering substantially better adhesion to the substrate material of the hemisphere (zirconia in our case) and, in addition, it forms a natural, transparent few-nanometer-thick layer of surface oxide protecting the coating from damage. We also tried silver coatings, which required a 20-nm layer of silica on top to protect silver from oxidation. However, we found the silver coating to be very fragile and prone to scratches and exfoliation, for which reasons we favoured titanium coatings.

We assume that all NV defects at the same depth below the diamond surface are equivalent except of their different spatial orientations. Therefore, instead of moving the spherical mirror to change the NV defect–mirror distance, we observed different areas within the NV-implanted region of the diamond to study the effect of LDOS variation on the decay rate [23]. This allowed us keeping the spherical mirror at a fixed position on top of the diamond sample, and we moved the diamond sample together with the mirror as a whole during measurements with the aid of a piezo stage. This approach yields several advantages compared to the arrangement exploited in [15], where a compact metal sphere was attached to the tip of a scanning near-field optical microscope operating in the shear-force feedback mode. Due to the nature of the shear-force feedback, the separation between the mirror and the sample can only be kept constant to a certain level of precision. Moreover, the contact scanning mode can leave scratches on the metal coating, which subsequently impacts the LDOS and introduces noise in the NV defect lifetime measurements. However, the approach in [15] is suitable for single NV interrogation which is not the case for the method we are using.

Our experimental setup is a conventional confocal microscope optimized for fluorescence lifetime imaging (FLIM). For excitation, we use a pulsed 532-nm laser that generates 4.6-ps-wide pulses at a repetition rate of 5 MHz and set to a relatively low average power of $\sim$ 50 μW. This power level is well below the fluorescence saturation power and only limited by the ne-

Optics EXPRESS

cessity to maintain a low count rate at the photo detector to avoid piling up of the counts [25]. Atop of the 0.3-mm-thick diamond sample we place a spherical metal mirror for the modification of the LDOS, while we access the defects through the diamond bottom surface for excitation and collection of fluorescence with a 60x objective that has a numerical aperture of 0.7 [Fig. 1(a)]. Diamond has a high refractive index of $n_d \sim 2.4$, which leads to strong reflections at the diamond-air interface along the pathway from NV defects to the metal mirror and backwards. These reflections were reduced by filling the air gap with a fluorescence-free immersion oil of refractive index $n_{oil} = 1.5$. To make confocal FLIM scans, we mount the sample on a three-dimensional piezo stage. Since the radius of the spherical metal mirror is substantially larger than the gap size, the illuminated NV defects within the collection spot of the confocal microscope are to a good approximation in a planar-geometry configuration and therefore experience the same LDOS, i.e., each pixel of the FLIM map represents multiple NV defects that have the same radiation properties. Given that the radius of the metal mirror is known, the obtained FLIM images are straightforward to convert to a dependence $\tau = \tau(d)$, where τ is the fluorescence lifetime of NV defects and d is the local depth of the metal mirror [see Fig. 1(a)].

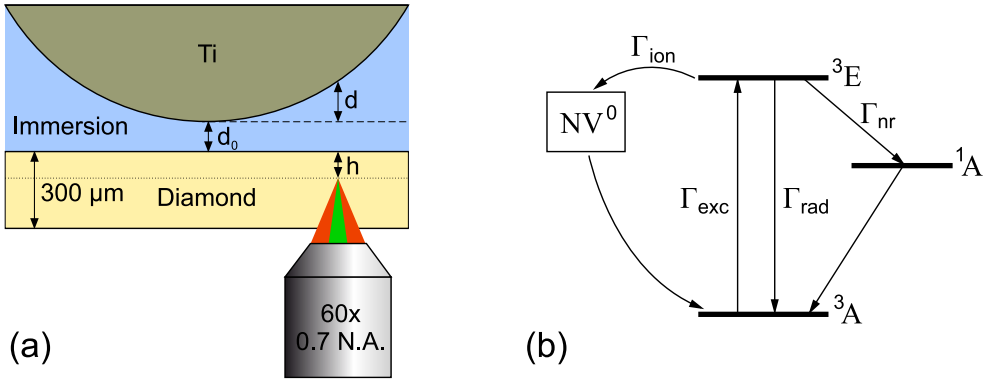

Fig. 1. (a) Schematics (not to scale) of the confocal arrangement with a spherical metal mirror to modify the LDOS of shallow implanted NV defects at depth h below the surface of a diamond plate. We investigated samples with $h = 4.5$ nm and 8 nm, respectively. (b) Illustration of the energy levels of the negatively-charged NV^- defect with an effective state for NV^0, which decreases the lifetime of the optically excited state due to a photoionization decay channel.

We note that the presence of the metal mirror modifies only the radiative part of the total decay rate by a factor F commonly referred to as the Purcell enhancement: $1/\tau(d) \equiv \tilde{\Gamma}_{tot} = F\Gamma_{rad} + \Gamma_{nr}$. The relative change in the total decay rate is then given by $\tilde{\Gamma}_{tot}/\Gamma_{tot} = 1 + \frac{\Gamma_{rad}}{\Gamma_{rad}+\Gamma_{nr}}(F-1)$, where the ratio before the brackets is the IQE η. Hence, we finally obtain:

$$\tilde{\Gamma}_{tot} = \Gamma_{tot}\left[1 + \eta(F-1)\right], \tag{1a}$$

or, equivalently:

$$\tau = \tau_0 / \left[1 + \eta(F-1)\right], \tag{1b}$$

where τ is the (mirror-affected) lifetime evaluated in the FLIM measurements of NV defects, whereas τ_0 is its unmodified value for defects in the absence of the metal mirror. We calculate the Purcell enhancement F as the ratio of total power radiated by a point dipole in a layered medium with a mirror at distance d to that of a point dipole in the same configuration but with a mirror at $d \to \infty$ and without immersion oil, carefully taking into account the actual distribution of dipole orientations in the crystal lattice with (100) top surface (see Appendix A). The calculated enhancement F is a function of the gap size d between the diamond sample and the metal mirror.

Optics EXPRESS

Finally, we can use Eq. (1) to fit the experimentally obtained dependence $\tau = \tau(d + d_0)$ using three fitting parameters: τ_0, η, d_0. Here, d_0 is the minimum gap size between the diamond and the sphere [Fig. 1(a)], which is introduced in our model to account for a possible slight elevation of the spherical mirror above the diamond surface due to the immersion oil.

Since in our study we focus on the properties of the emitter itself, we denote radiative decays Γ_{rad} as those due to the direct transition from the NV excited triplet state ^3E to the ground state ^3A, irrespective of whether it results in a detectable photon or in excitation of surface states of the metal mirror [26, 27]. Such surface states can be surface plasmon polaritons or high-wavenumber plasmon modes — processes sometimes classified as fluorescence quenching. The latter becomes the dominating decay channel for an emitter near a metal surface. Owing to near-field energy transfer (see Appendix A) it occurs when the separation is $\lesssim \lambda/10$ [28,29], where λ is the emission wavelength in the emitter's medium. Note that truly non-radiative quenching mechanisms such as charge transfer to the metal do not play a role in our system because the NV defects reside at least 4.5 nm away from the metal. Correspondingly, we consider non-radiative decays to be due to the internal structure of the NV defect such as vibrational relaxation and intersystem crossing. According to the above conventions, the Purcell enhancement is defined as an increase in the radiative decay rate. From Eq. (1b), one notices that for the particular case of an emitter with IQE equal to unity, i.e., when non-radiative decays can be neglected, $\tau_0/\tau = F$.

3. Experimental results

Using a scanning piezo stage, we translate the sample together with the spherical metal mirror on top [Fig. 1(a)] relative to the stationary laser beam in order to obtain confocal fluorescence [Fig. 2(a)] and lifetime [Fig. 2(b)] maps of the sample (for details on lifetime measurements, see Appendix A). As expected and similar to the results in [15], the fluorescence image consists of concentric rings whose geometry and origin are the same as in Newton's rings experiment. The noticeable straight lines that go across the fluorescence image correspond to scratches on the diamond surface caused by the mechanical polishing process. Those imperfections as well as several other irregularities have a slight impact on the lifetime measurement results and hence we exclude those points in our data analysis. The confocal FLIM map of the sample [Fig. 2(b)], similar to the fluorescence image, consists of concentric rings implying that the lifetime of NV defects oscillates with increasing emitter-to-mirror separation due to a varying LDOS. In order to interpret the results, we convert coordinates of the points on the FLIM map into the equivalent gap size d, then average the lifetime values for the points corresponding to the same gap, and plot the obtained data as a dependence of lifetime on the gap size. This has been done for NV defects implanted 4.5 nm [Fig. 3(a)] and 8 nm [Fig. 3(b)] below the diamond surface.

For a simple system, where the lifetime is only affected by LDOS modifications, one would expect to observe smooth decaying periodic oscillations of the lifetime with an increased emitter-to-mirror distance (e.g., cf. [30]). Contrary, our data show broken periodicity in oscillations with jumping amplitude, a feature akin to beating of several periodic signals. Indeed, Fourier analysis of many lifetime-vs-distance profiles revealed strong contributions at two Fourier frequencies [Fig. 3(c)]: one at a corresponding wavelength of around 690 nm, the room-temperature fluorescence maximum of NV defects, and another at around 532 nm. Note that due to the limited number of experimental points and the discrete nature of the applied Fourier transformation, the maxima in the Fourier spectrum in Fig. 3(c) are not well defined. However, in a series of repeated measurements we consistently observe two major peaks in the Fourier spectrum, revealing a somewhat unexpected contribution at a frequency corresponding to the excitation wavelength. This additional contribution makes fitting of the experimental results with Eq. (1b) satisfactory only within the first 500–1000 nm of the gap size, becoming often in counter-phase with the oscillations for separations $d > 1000$ nm. Note that this might

Optics EXPRESS

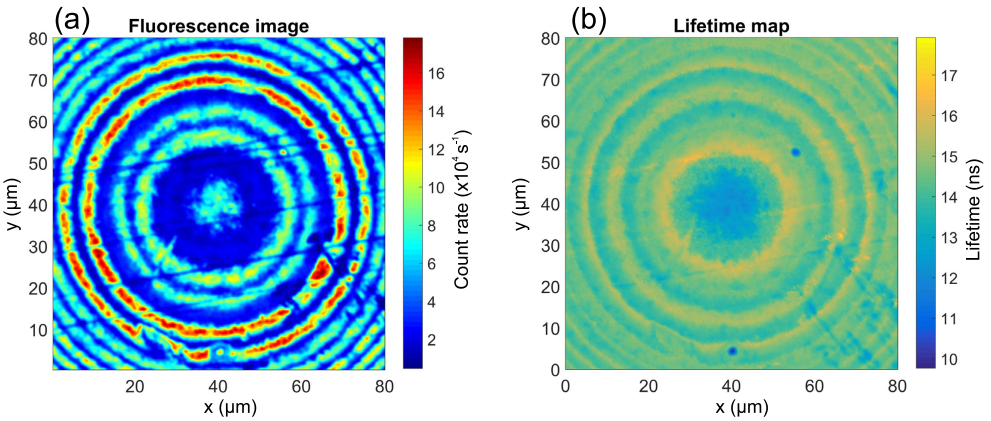

Fig. 2. (a) Fluorescence map recorded in a confocal scan of NV defects implanted 8 nm below the diamond surface. (b) Fluorescence lifetime map obtained by single-exponential fitting of confocal lifetime data recorded simultaneously with the fluorescence map shown in panel (a).

have also been the case in [15].

Our observations suggest that the lifetime of NV defects depends on the excitation light intensity. The additional contribution can indeed be explained by taking into account an intensity dependent transition to another level, presumably a photo-induced ionization process of negatively charged NV defects [31, 32]. Transitions to the neutral-charge state NV^0 at a rate Γ_{ion} provide an additional decay channel for the excited state ^3E of the NV^- defect, effectively decreasing its lifetime [Fig. 1(b)]. The photoionization dynamics of NV defects have recently been studied in detail [33], and the ionization energy was determined to be 2.60 eV. Since our excitation energy per photon at 532 nm is below that, the photoionization in our case is a two-photon process, and hence Γ_{ion} scales quadratically with the excitation intensity [33]. To address photoionization in the fitting procedure, we modify Eq. (1a) by adding an ionization decay channel to the total decay rate:

$$\tilde{\Gamma}_{tot} = \Gamma_{tot}\,[1 + \eta(F-1)] + bI_{exc}^2, \tag{2}$$

where b is a fitting parameter and the excitation intensity I_{exc} is given by the Newton's rings interference pattern: $I_{exc} = \sin^2[2\pi n_{oil}(d+d_0)/\lambda]$ with $\lambda = 532$ nm and $n_{oil} = 1.5$. This yields the following fitting Eq. for the lifetime:

$$\tau = \tau_0 / \left[1 + \eta(F-1) + \tau_0 b I_{exc}^2\right]. \tag{3}$$

Note that even though there are now four fitting parameters, they all have an independent impact on the measurement outcome and the fitting procedure converges quickly. The vertical position of oscillations relative to the y-axis in Figs. 3(a) and 3(b) is determined by τ_0, while η determines the oscillation amplitude, d_0 is the horizontal displacement of the oscillations along the x-axis, and b is the value of the harmonic distortion, which shows the amount of contribution of the intensity signal [Fig. 2(a)] to the FLIM map [Fig. 2(b)].

We apply this fitting procedure to measurements at two different areas on the sample with NV defects implanted 4.5 and 8 nm below the diamond surface [lines on Figs. 3(a) and 3(b)]. There are two main sources of errors in obtaining the values of the fitting parameters: uncertainty in exponential decay fitting while obtaining lifetime values for the FLIM map and error of fitting the final data with Eq. (3). We repeated measurements with the two implanted areas several times also by replacing the mirror, which gave very good reproducibility within the interval of the fitting errors. The obtained fitting parameters are presented in Table 1 and were obtained

Optics EXPRESS

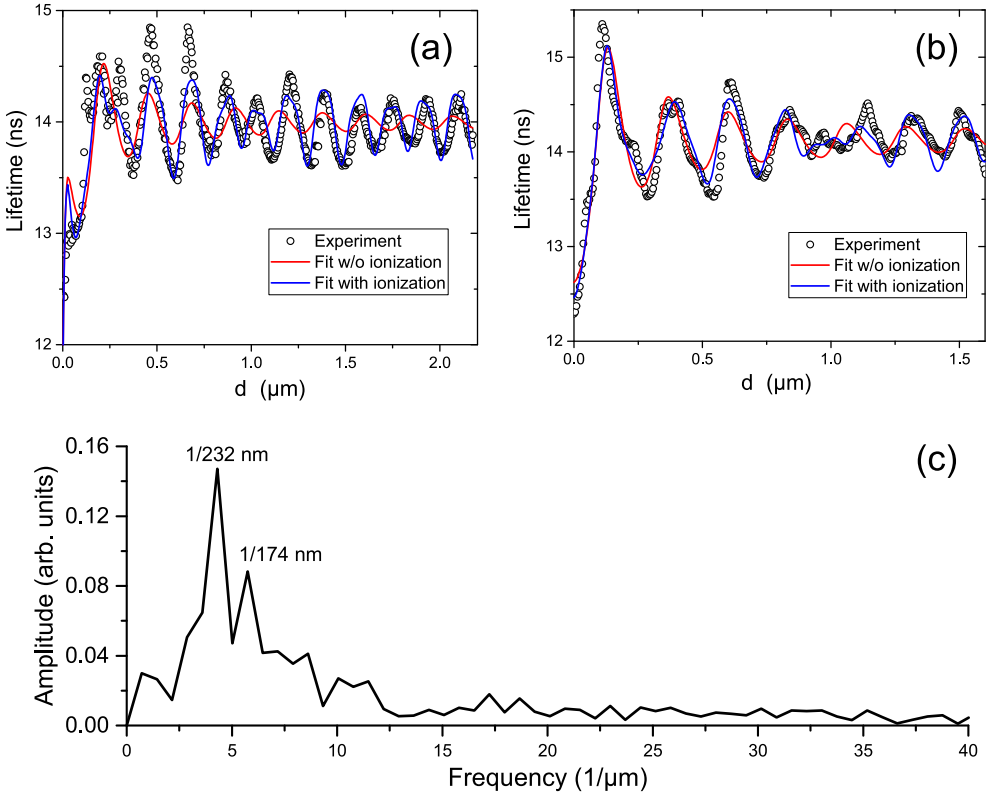

Fig. 3. (a) and (b) Dependence of fluorescence lifetime on the gap size derived from respective FLIM maps by averaging through pixels corresponding to the same gap size d. Dots show experimental data points, red curve — fit with Eq. (1), blue curve — fit with Eq. (3) that takes into account photo-induced ionization of NV defects. Dependence shown for (a) 4.5- and (b) 8-nm-deep implanted NV defects. (c) An example of Fourier transformation of lifetime vs. gap size dependence that reveals the dominating periods (here 174 nm and 232 nm) given by $\lambda/(2n_{oil})$.

through averaging several (three and two for 4.5- and 8-nm-deep NV defects, respectively) experimental runs, except d_0, which varied from trial to trial and was typically within the interval 20–100 nm.

Table 1. (columns 1–3): experimental fitting parameters (averaged through repeated measurements) for Eq. (3) giving the best fit to data shown on Figs. 3(a) and 3(b); (columns 4–6): radiation parameters derived from the fitting parameters.

Depth	η	τ_0, ns	b, μs^{-1}	Γ_{rad}, μs^{-1}	Γ_{nr}, μs^{-1}	τ_{bulk}, ns
4.5 ± 1 nm	0.70 ± 0.07	14.9 ± 0.5	2.3 ± 0.9	47 ± 5	20 ± 2	11.6 ± 0.8
8 ± 2 nm	0.82 ± 0.08	15.0 ± 0.5	2.2 ± 0.6	55 ± 6	12 ± 1	11.4 ± 0.8

The obtained mean values of quantum efficiency are 0.70±0.07 and 0.82±0.08 for ensembles of NV defects implanted 4.5 and 8 nm below the diamond surface, respectively. From the values η and τ_0 we can directly calculate the radiative and non-radiative decay rates of NV defects at the corresponding depths: $\Gamma_{rad} = \eta\Gamma_{tot} \equiv \eta/\tau_0$ and $\Gamma_{nr} = \Gamma_{tot} - \Gamma_{rad}$. As expected, the radiative decay rate increases slightly for deeper implantation (Tab. 1) as a result of an increased

Optics EXPRESS

effective refractive index (and hence LDOS) surrounding the emitters. In contrast to this, the non-radiative decay rate decreases almost by half. We speculate that this is likely due to a decreased surface strain in the diamond or other surface related non-radiative decay channels. We note that a similar observation has been reported in [15], where NV defects inside the smallest diamond nanocrystals were measured to have the largest non-radiative decay rate. Since the variation of non-radiative decay rate with depth is difficult to address analytically, we cannot extrapolate precisely the obtained values to NV defects deep inside a bulk diamond. However, if we disregard a change of Γ_{nr} with depth and apply Eq. (1b) to the obtained fitting parameters (separately for the values obtained for 4.5 and 8 nm implantation depth, respectively) we can estimate the lifetime of deep NV defects. Noticeably, the estimated lifetime values of deep NV defects, 11.6 ns and 11.4 ns, are close to those measured for the spin-zero excited state [34–36]. This indicates that (*i*) our assumption is a fair approximation and the Γ_{nr} is unlikely to decrease substantially further for NV defects located deeper than 8 nm under the diamond surface, and (*ii*) in our measurements we have substantial spin polarization. Making another realistic assumption that the non-radiative decay rate can only decrease with the NV defect located deeper in the diamond, we can make a lower estimation of the IQE of the defect in bulk diamond: assuming that the non-radiative decay rate is similar to the value for 8-nm-deep NV defects: $\Gamma_{rad}^{bulk} \gtrsim 1/\tau_{bulk} - \Gamma_{nr}^{8nm} = 76\ \mu\text{s}^{-1}$, we estimate $\eta_{bulk} = \Gamma_{rad}^{bulk}\tau_{bulk} \gtrsim 0.86$.

To conclude, we consistently performed reproducible measurements of the lifetime of NV defects implanted 4.5 and 8 nm below the diamond surface as a function of distance to a metallic mirror. By fitting to a well-established model we confirm that the NV defect in diamond is indeed a bright source of photons with high IQE of more than 70%. Using two fair approximations that find support in the experiment, we extrapolated the IQE and total fluorescence lifetime to NV defects in bulk diamond and found those values to be $\gtrsim 0.86$ and ~ 11.4 ns, respectively. In fitting the experimental data, we used a model that takes into account a photo-induced relaxation process, which we assumed to be photoionization of negatively charged NV defects to the neutral-charge state. We showed that this process cannot be neglected and plays a noticeable role in the modification of the decay rate. The applied model of two-photon ionization is a simplification and does not account for the reverse process of photo-induced recombination. Due to the nature of the experimental technique, it is not suitable for the study of luminescence defects located substantially deeper below the surface than what we have measured here. On the other hand, our measurements combined with techniques for spin-state preparation of the NV defect, can yield more information about rates of particular transitions. Furthermore, the technique could be successfully applied for the investigation of other highly promising but substantially less studied Si- and Ge-vacancy defects in diamond.

Appendix A

Given that the radius of the metallic mirror (1000 μm) is much larger than its separation from NV defects (typically below 1 μm), we can consider radiating NV defects as electric dipoles located close to an interface with planar stratified media. Light emission by point dipoles in such a configuration has been studied in details by Lukosz and Kunz [28]. Following their technique, the Purcell factor F can be calculated as the ratio of the total power radiated by an ensemble of electric dipoles close to stratified media (formed by diamond, metal mirror, and a gap between them filled with an immersion oil) to that radiated by the same ensemble with the metallic mirror and oil removed from the diamond surface, i.e. near the semi-infinite media of diamond and air. In order to evaluate contributions of dipoles with different orientations to the full ensemble, we have to consider a distribution of electric dipoles of NV defects in the diamond crystal lattice.

The emission from the NV defect is due to one of the two possible electric dipole transitions, which are orthogonal to each other and located in the plane perpendicular to the symmetry axis (z axis) of the NV defect [37,38]. The particular orientation of the dipoles is determined by non-

Optics EXPRESS

axial local strain, and can be assumed to be distributed homogeneously in the xy plane for a large ensemble of NV defects. Taking into account the four possible orientations of NV defects in the diamond crystal lattice — [111], [$\bar{1}\bar{1}$1], [$\bar{1}$1$\bar{1}$], and [1$\bar{1}\bar{1}$] — we derive the following relative amount of parallel and perpendicular dipoles in the ensemble with respect to the (100) surface plane:

$$a_{\parallel} = \frac{1+\cos\theta}{1+\cos\theta+\sin\theta}, a_{\perp} = \frac{\sin\theta}{1+\cos\theta+\sin\theta}, \tag{4}$$

where $\theta = \tan^{-1}\sqrt{2} \approx 54.7°$ is the half-angle between the neighbouring bonds. This results in $a_{\parallel} \approx 0.659$ and $a_{\perp} \approx 0.341$, very close to the values corresponding to a homogeneous distribution of dipoles with $a_{\parallel} = 2/3$ and $a_{\perp} = 1/3$. The latter result is not surprising, given that the four possible orientations of the NV defect homogeneously fill the full 4π solid angle, forming a very symmetric tetrahedral arrangement.

In calculation of the Purcell factor $F(d)$, we consider two semi-infinite diamond and titanium media separated by a planar gap of variable thickness d. The refractive index of diamond is taken to be $n_d = 2.41$, the dielectric constant of titanium ($\varepsilon = -7.3847+22.194i$) is from Johnson and Christy [39] at a wavelength of 690 nm — the approximate center of the NV defect fluorescence spectrum, and the refractive index of the gap filled with immersion oil is $n_{oil} = 1.5$.

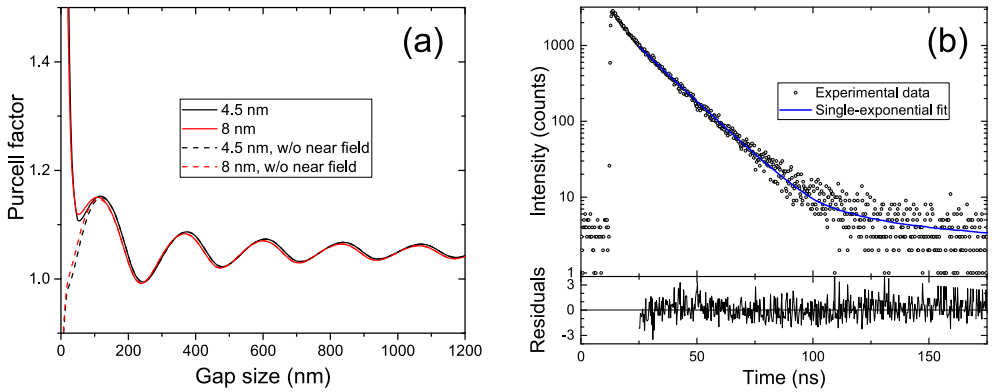

Fig. 4. (a) Purcell factor calculated for an ensemble of 4.5- and 8-nm-deep implanted NV defects in bulk diamond.(b) An example of lifetime histogram with the best fit curve and normalized fitting residuals.

The resulting calculated Purcell factor for 4.5- and 8-nm-deep NV defects is plotted in Fig. 4(a) (solid lines). Since we defined the Purcell factor relative to the NV defect located near the diamond-air interface, the decaying periodic oscillations tend to a value above unity for the infinite gap size, because the effective refractive index (and hence the LDOS) around the dipole is increased by substituting air with oil. For the limit of a vanishing gap, the Purcell enhancement increases drastically because of the near-field energy transfer to free electrons in metal, where the local density of states is very high. Interestingly, if we disregard the near-field part of the dipole radiation, the trend for Purcell enhancement at zero-size gap will change to the opposite [dashed lines in Fig. 4(a)]. Indeed, a metallic mirror efficiently reflects incident far-field radiation, introduces an additionally π phase shift such that the reflected field interferes destructively with the incident field. This inhibits radiation from the dipole and reduces the radiative decay rate.

We performed fluorescence lifetime measurements using the time-correlated single-photon counting technique. The accumulation of data for each point was continued until at least 1000 counts were detected at the maximum of the lifetime histogram. Depending on the photon count rate, the dwell time at each point of the FLIM image could vary from 2 to 30 seconds, such that

Optics EXPRESS

the overall acquisition time of one image was up to two days. This required high mechanical and thermal stability of the setup. To evaluate the lifetime, we accomplished tail fitting of the histogram data with a single-exponent decay function, leaving out the first 10 ns of the time trace to exclude the influence of the instrument-response function. Single-exponent fitting provided satisfactory results with the normalized residuals being in the range $[-3; 3]$ and typically within $[-2; 2]$. A representative lifetime histogram together with the fit curve and normalized residuals of the fitting is shown in Fig. 4(b). These data were taken near the first bright ring of the FLIM image shown in Fig. 2(b) with the fitted lifetime being 14.9 ns.

Funding

This work is supported by the Innovation Foundation Denmark with the project EXMAD and the Danish Research Council through the Sapere Aude project DIMS.

Acknowledgments

The authors acknowledge the FLIMfit software tool developed at Imperial College London.